Journal of Mechanics Engineering and Automation 7 (2017) 209-220
doi: 10.17265/2159-5275/2017.04.005

Stress Analysis of a Circularly-Perforated Finite Orthotropic Composite Plate

N. Fatima and R. Rowlands

Department of Mechanical Engineering, University of Wisconsin-Madison, Madison, WI 53706, USA

Abstract: Stresses, particularly those at geometric discontinuities, can influence structural integrity of engineering components. Motivated by the prevalence of cutouts in components, the objective of this paper is to demonstrate ability to stress analyze finite, circularly-perforated orthotropic composites whose external loading may be unknown. Recognizing difficulties in obtaining purely theoretical or numerical solutions, the paper presents a hybrid means of stress analyzing such structures. Individual stresses, including those on the edge of the hole, are obtained in a loaded finite graphite/epoxy composite tensile plate containing a round hole by processing measured values of a single displacement field with an Airy stress function in complex variables. Displacements are recorded by digital image correlation. Traction-free conditions are satisfied analytically at the edge of the hole using conformal mapping and analytic continuation. Stresses satisfy equilibrium and strains satisfy compatibility. Significant features of the technique include its wide applicability, it smooths the measured information, does not require knowing the applied loading, and the rigorous mechanics foundation by which strains are determined from measured displacements.

Key words: Stress analysis, composites, experimental mechanics, orthotropy, DIC (digital image correlation).

List of Symbols

a_{ij}	Elastic compliances
a_j, b_j	Real coefficients
c_j	Complex coefficients
B, C	Complex material quantities
d	Recorded displacements
d’	Reconstructed displacements
D	Hole diameter
E_{xx}, E_{yy}	Elastic moduli
F	Airy stress function
F*	Applied load
G_{xy}	Shear modulus
h	Number of imposed condition
k	Number of complex coefficients
L	Length of the plate
m	Integers for range of the summation series
n	Number of input measured displacements
p_j, q_j	Material properties
R	Hole radius
t	Plate thickness
u, v	Cartesian displacement components
W	Width
x, y	Rectangular coordinates in physical plane
z_j	Complex variable
ζ	Complex plane
μ	Complex material properties
ν_{xy}	Poisson’s ratio
ξ, η	Complex coordinates in mapped plane
σ_0	Far-field stress
σ_{xx}, σ_{yy}, σ_{xy}	Cartesian stress components
σ_{rr}, $\sigma_{\theta\theta}$, $\sigma_{r\theta}$	Polar stress components
Φ, Ψ	Airy stress functions
ω	Mapping function

Corresponding author: R. E. Rowlands, Ph.D., emeritus professor, research fields: experimental mechanics and composite materials.

1. Introduction

The objective of this study is to demonstrate the ability to determine the individual stresses full-field in a circularly-perforated, finite orthotropic composite plate (Fig. 1) from recorded information of a single displacement component and without requiring knowledge of the external loading.

High strength- and stiffness-to-weight ratios often make composite materials popular over isotropic, monolithic materials. Moreover, composite structures containing geometric discontinuities are prevalent load bearing components. Structural integrity is influenced

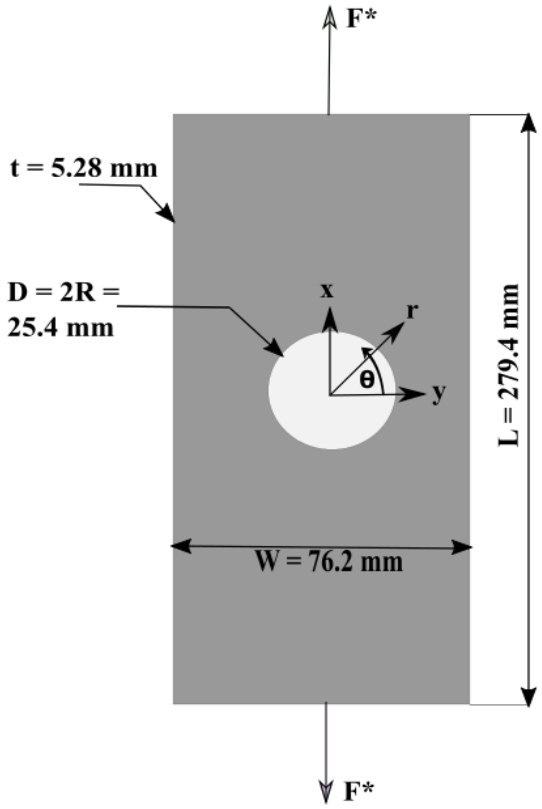

Fig. 1 Loaded [$0_{13}/90_5/0_{13}$] graphite/epoxy laminated plate.

by the stresses. While extensive stress information associated with geometric discontinuities is available for isotropic materials, relatively little such data exist for orthotropic materials [1]. Stresses in composite structures depend on the material properties. Anisotropy often complicates the stress distributions near geometric discontinuities. The orthotropic behavior can influence where along the boundary of a hole the most serious stresses occur, something that one need not know a priori [2, 3]. Few theoretical analyses of finite orthotropic structures having cutouts are available. Like numerical analyses, they require knowing the boundary conditions. The latter are often unknown in practice. Purely experimental techniques do not tend to provide reliable data near the edge of a geometric discontinuity. Moreover, traditional displacement-based experimental methods of stress analysis have the additional challenge of having to differentiate the displacement data to obtain stresses. Differentiating measured information can be unreliable. Recognizing these difficulties, this paper utilizes a complex variable method to perform full-field stress analysis of a loaded finite orthotropic plate containing a central circular hole from recorded data of a single component of displacement. Needing only one displacement field can be advantageous. For example, situations may occur where there is a paucity or inferior quality of one or other of the in-plane displacements.

The present hybrid method of combining recorded displacement data, conformal mapping, analytic continuation, an Airy stress function and least squares is effective for stress analyzing perforated finite orthotropic structures without requiring knowledge of external loading conditions. The DIC (digital image correlation)-measured displacements in the loading direction are processed here with a series representation of an Airy stress function in complex variables. The present technique simultaneously smooths the measured displacement data, satisfies equilibrium and compatibility, and determines individual stresses full-field, including on the edge of the hole. Knowing the independent stresses is necessary if fatigue or strength criteria are involved. The approach also benefits from the rigorous mechanic's foundation by which strains are determined from measured displacement data. Reliability is demonstrated by FEM (finite element method) and force equilibrium. The authors are unaware of any published stresses at a hole in an orthotropic composite from a DIC-recorded single displacement field.

2. Literature Review

Lagattu et al. [4] and Ashrafi and Tuttle [5] are seemingly the only prior publications which employ DIC-measured displacement information to stress analyze orthotropic composites containing a round hole. These analyses necessitated measured values of both in-plane displacement components and experienced difficulties in obtaining reliable result on

the edge of the hole. Ref. [4] also did not provide the three individual components of strain or stress full-field.

3. Relevant Equations

The Airy stress function for orthotropic materials can be expressed as Ref. [6].

$$F = 2Re[F_1(z_1) + F_2(z_2)] \quad (1)$$

where, $z_j = x + \mu_j y$ for j = 1, 2. $F_1(z_1)$ and $F_2(z_2)$ are analytical functions of the complex variables z_1 and z_2, respectively, and "Re" represents the real part of the complex quantities. Relative to the principal axes of orthotropy, the complex material properties, μ_j, are the roots of the following characteristic equation.

$$a_{11}\mu^4 + (2a_{12} + a_{66})\mu^2 + a_{22} = 0 \quad (2)$$

where, a_{ij} are the following elastic compliances.

$$a_{11} = \frac{1}{E_x}, a_{12} = \frac{-v_{yx}}{E_y}, a_{22} = \frac{1}{E_y} \; and \; a_{66} = \frac{1}{G_{xy}}$$

Knowing the orthotropic constitutive properties, μ_1 and μ_2 are known. Stresses and in-plane displacements in rectangular coordinates (x, y) of the physical plane, z = x + iy, can be expressed as:

$$\sigma_{xx} = 2Re[\mu_1^2\Phi'(z_1) + \mu_2^2\Psi'(z_2)] \quad (3)$$

$$\sigma_{yy} = 2Re[\Phi'(z_1) + \Psi'(z_2)] \quad (4)$$

$$\sigma_{xy} = -2Re[\mu_1\Phi'(z_1) + \mu_2\Psi'(z_2)] \quad (5)$$

$$u = 2Re[p_1\Phi(z_1) + p_2\Psi(z_2)] \quad (6)$$

$$v = 2Re[q_1\Phi(z_1) + q_2\Psi(z_2)] \quad (7)$$

where, $\Phi(z_1) = \frac{dF_1(z_1)}{dz_1}$, $\Psi(z_2) = \frac{dF_2(z_2)}{dz_2}$ and the primes represent differentiation with respect to the complex variable z_j. In the above equations, u is the displacement in the direction of loading (x-direction) and v is that in the y-direction. With respect to the directions of material symmetry, the variables p_1, p_2, q_1 and q_2 are:

$$p_1 = a_{11}\mu_1^2 + a_{12}$$
$$p_2 = a_{11}\mu_2^2 + a_{12}$$
$$q_1 = a_{12}\mu_1 + \frac{a_{22}}{\mu_1} \quad (8)$$
$$q_2 = a_{12}\mu_2 + \frac{a_{22}}{\mu_2}$$

Since the $[0_{13}/90_5/0_{13}]$ graphite/epoxy plate of Fig. 1 is a balanced, symmetric construction, the displacements and strains are uniform through the thickness. The measured in-plane laminate elastic properties and the stresses of Eqs. (3)-(5) are based on average stresses through the thickness.

Using conformal mapping and analytic continuation in regions adjacent to the traction-free edge of a cutout, the stress functions $\Phi(z_1)$ and $\Psi(z_2)$ can be related to each other. The stresses may then be expressed using only one stress function. The stress functions are expressible as power series expansions whose unknown complex coefficients can be determined experimentally. Knowing the complex coefficients, the stress functions $\Phi(z_1)$ and $\Psi(z_2)$ are evaluated from which the individual stresses are available from Eqs. (3)-(5).

Using a mapping function, a region of a simpler shape in the $\zeta = \xi + i\eta$ plane can be mapped into a comparatively complicated region in the physical plane z = x + iy of the loaded structure, Fig. 2. The auxiliary planes are expressed as $\zeta_j = \xi + \mu_j\eta$ and the mapping function is:

$$z_j = \omega_j(\zeta_j) \quad (9)$$

The stress functions $\Phi(z_1)$ and $\Psi(z_2)$ can be expressed as analytical functions of ζ_1 and ζ_2.

$$\Phi(z_1) = \Phi[\omega_1(\zeta_1)] \equiv \Phi(\zeta_1) \quad (10)$$

$$\Psi(z_2) = \Psi[\omega_2(\zeta_2)] \equiv \Psi(\zeta_2) \quad (11)$$

and

$$\Phi'(z_1) = \Phi'(\zeta_1)\frac{d\zeta_1}{dz_1} = \frac{\Phi'(\zeta_1)}{\omega_1'(\zeta_1)} \quad (12)$$

$$\Psi'(z_2) = \Psi'(\zeta_2)\frac{d\zeta_2}{dz_2} = \frac{\Psi'(\zeta_2)}{\omega_2'(\zeta_2)} \quad (13)$$

where

$$\frac{dz_j}{d\zeta_j} = \omega_j'(\zeta_j) \quad (14)$$

Substituting Eqs. (12)-(14) into Eqs. (3)-(5) gives

$$\sigma_{xx} = 2Re\left[\mu_1^2\frac{\Phi'(\zeta_1)}{\omega_1'(\zeta_1)} + \mu_2^2\frac{\Psi'(\zeta_2)}{\omega_2'(\zeta_2)}\right] \quad (15)$$

$$\sigma_{yy} = 2Re\left[\frac{\Phi'(\zeta_1)}{\omega_1'(\zeta_1)} + \frac{\Psi'(\zeta_2)}{\omega_2'(\zeta_2)}\right] \quad (16)$$

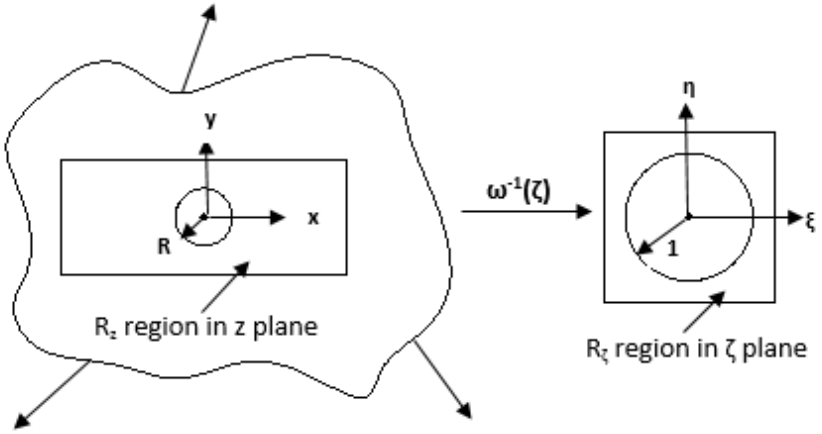

Fig. 2 Mapping edge of circular hole from physical z-plane to unit circle in ζ-plane.

$$\sigma_{xy} = -2Re\left[\mu_1 \frac{\Phi'(\zeta_1)}{\omega_1'(\zeta_1)} + \mu_2 \frac{\Psi'(\zeta_2)}{\omega_2'(\zeta_2)}\right] \tag{17}$$

In regions adjacent to a traction-free-boundary, the technique of analytic continuation enables the previous two stress functions to be expressed in terms of each other [7], i.e.,

$$\Psi(\zeta_2) = B\overline{\Phi(\bar{\zeta}_2)} + C\Phi(\zeta_2) \tag{18}$$

where B and C are

$$B = \frac{\bar{\mu}_2 - \bar{\mu}_1}{\mu_2 - \bar{\mu}_2} \;\; and \;\; C = \frac{\bar{\mu}_2 - \mu_1}{\mu_2 - \bar{\mu}_2} \tag{19}$$

The individual stresses can now be written in terms of the single function $\Phi(\zeta_j)$. It is convenient to express the latter as a Laurent series such that the boundary of the hole of radius R in the physical plane is mapped into the unit circle in the complex ζ-plane, Fig. 2, i.e.,

$$\Phi(\zeta_1) = \sum_{\substack{j=-m \\ j\neq 0}}^{j=m} c_j \zeta_1^j \tag{20}$$

$$\Psi(\zeta_2) = \sum_{\substack{j=-m \\ j\neq 0}}^{j=m} \left(\bar{c}_j B \zeta_2^{-j} + c_j C \zeta_2^j\right) \tag{21}$$

The Airy coefficients c_j are complex numbers, i.e., $c_j = a_j + ib_j$, where, a_j and b_j are real numbers. B and C are given by Eq. (19). For the central hole, and due to the symmetry, the value of j is never zero or an even number.

Combing Eqs. (6), (7), (20) and (21) provides the following expressions for the displacements.

$$u = 2Re\left(\sum_{\substack{j=-m \\ j\neq 0}}^{j=m} \left\{\left[p_1\zeta_1^j + p_2\left(C\zeta_2^j + B\zeta_2^{-j}\right)\right]a_j + i\left[p_1\zeta_1^j + p_2\left(C\zeta_2^j - B\zeta_2^{-j}\right)\right]b_j\right\}\right) \tag{22}$$

$$v = 2Re\left(\sum_{\substack{j=-m \\ j\neq 0}}^{j=m} \left\{\left[q_1\zeta_1^j + q_2\left(C\zeta_2^j + B\zeta_2^{-j}\right)\right]a_j + i\left[q_1\zeta_1^j + q_2\left(C\zeta_2^j - B\zeta_2^{-j}\right)\right]b_j\right\}\right) \tag{23}$$

Eqs. (15)-(17) involve derivatives of the stress functions and these are:

$$\Phi'(\zeta_1) = \sum_{\substack{j=-m \\ j\neq 0}}^{j=m} j c_j \zeta_1^{j-1} \tag{24}$$

$$\Psi'(\zeta_2) = \sum_{\substack{j=-m \\ j\neq 0}}^{j=m} \left(-j\bar{c_j}B\zeta_2^{-j-1} + jc_jC\zeta_2^{j-1}\right) \tag{25}$$

Combing Eqs. (15)-(17) with Eqs. (24) and (25) gives

$$\sigma_{xx} = 2Re\left(\sum_{\substack{j=-m \\ j\neq 0}}^{j=m}\left[\mu_1^2\frac{jc_j\zeta_1^{j-1}}{\omega_1'(\zeta_1)} + \mu_2^2\frac{-j\bar{c_j}B\zeta_2^{-j-1} + jc_jC\zeta_2^{j-1}}{\omega_2'(\zeta_2)}\right]\right) \tag{26}$$

$$\sigma_{yy} = 2Re\left(\sum_{\substack{j=-m \\ j\neq 0}}^{j=m}\left[\frac{jc_j\zeta_1^{j-1}}{\omega_1'(\zeta_1)} + \frac{-j\bar{c_j}B\zeta_2^{-j-1} + jc_jC\zeta_2^{j-1}}{\omega_2'(\zeta_2)}\right]\right) \tag{27}$$

$$\sigma_{xy} = -2Re\left(\sum_{\substack{j=-m \\ j\neq 0}}^{j=m}\left[\mu_1\frac{jc_j\zeta_1^{j-1}}{\omega_1'(\zeta_1)} + \mu_2\frac{-j\bar{c_j}B\zeta_2^{-j-1} + jc_jC\zeta_2^{j-1}}{\omega_2'(\zeta_2)}\right]\right) \tag{28}$$

For the circularly perforated orthotropic plate, the conformal transformation from a unit circle in the ζ-plane to a circular hole of radius R in the physical z-plane is:

$$z_j = \omega_j(\zeta_j) = \frac{R}{2}\left[(1-i\mu_j)\zeta_j + \frac{1+i\mu_j}{\zeta_j}\right] \tag{29}$$

The inverse of Eq. (29) maps the round hole of radius R from the physical z-plane to the unit circle in the ζ-plane, i.e.,

$$\omega^{-1}(z_j) = \zeta_j = \frac{z_j \pm \sqrt{z_j^2 - R^2(1+\mu_j^2)}}{R(1-i\mu_j)}; j = 1,2 \tag{30}$$

The branch of the square root of the above equation is chosen so that, $|\zeta_j| \geq 1$. Eqs. (26)-(28) use the derivative of the mapping function $\omega_j(\zeta_j)$ with respect to the variable ζ_j, which is given by:

$$\omega_j'(\zeta_j) = \frac{R}{2}\left[(1-i\mu_j) - \frac{1+i\mu_j}{\zeta_j^2}\right]; j = 1,2 \tag{31}$$

4. Material Properties

The plate of Fig. 1 is an orthotropic $[0_{13}/90_5/0_{13}]$ graphite/epoxy laminate (from Kinetic Composites, Inc., Oceanside, CA). Measured laminate material properties are E_{xx} = 104.1 GPa, υ_{xy} = 0.16, E_{yy} = 28.1 GPa and G_{xy} = 3.0 GPa [8].

5. Plate Machining and Loading

The centrally circularly perforated, finite-width composite plate of Fig. 1 was waterjet-machined [8]. The plate was loaded in an MTS machine from 0 to 11.6 kN (2,600 lbs) in 889.6 N (200 lbs) increments. Reported results are for F* = 4.45 kN (1,000 lbs).

6. DIC [8-11]

DIC was used to measure the displacement information. Table 1 contains the DIC details**.** The surface of the plate was initially painted black, after which white speckles were applied.

The prepared plate was incrementally loaded in its strong/stiff x-direction in a 90 kN (20,000 lbs) capacity, hydraulic-grip MTS machine. Three-dimensional (both in-plane plus the out-of-plane) displacements were recorded using two cameras and ambient room lighting. The out-of-plane displacement information was monitored to ensure no out-of-plane motion occurred beyond the Poisson's effect. An image of the plate was recorded at each load level using the DIC system

(Correlated Solutions Inc., Columbia, SC 29063, USA). While the displacements were recorded with the Correlated Solutions' Vic-Snap software, these measured u-displacements were processed into strains using the Airy stress function rather than the commercially-provided system. The v-displacement information was not explicitly utilized.

The measured DIC data were combined with the stress function to determine the stresses. Although the recorded displacement information at, and adjacent to, an edge is unreliable and raw displacement information in composites tends to be inherently noisy, the present technique overcomes these challenges by avoiding the use of recorded displacement data at and near edges and by processing the measured data away from edges using an Airy stress function, mapping and analytic continuation. The magnitudes of the finite number of Airy coefficients utilized were determined from the measured displacements. The resulting reliable DIC-determined stresses are available on, and in the neighborhood of the edge of the hole without having to know the distant geometry or loading.

7. Finite Element Analysis

A motivation for developing the present hybrid technique is to enable stress analyzing perforated orthotropic cases experimentally which cannot be analyzed numerically (e.g., inadequate knowledge of the external loads), yet FEM is used here. However, the present geometry and loading were selected so that one could obtain reliable FEM results with which to compare those of the hybrid method.

Having geometric and loading symmetry about both the x and y axes, only one quarter of the plate was modeled numerically using the commercial FE program ANSYS APDL. ANSYS elements plane 182 (4 nodes and 2 degrees of freedom) were employed. The geometry was modeled with the origin of the coordinate systems at the center of the hole. Symmetry boundary conditions were imposed. A high mesh density was utilized near the hole. A far-field stress of σ_0 = 11.05 MPa (1,603 psi) was applied in the x-axis (strong-stiff direction) based on the applied load and the far-field cross-sectional area of the plate, Eq. (32). The quarter-plate model consists of 26,000 elements and 26,371 nodes. The x-y coordinates of all the nodes, along with the displacement and stress components, were imported into Matlab for post-processing and correlating the FEA predictions with those from the DIC-hybrid analysis. Ref. [8] contains the FEM details.

$$\sigma_0 = \frac{F^*}{Wt} = \frac{4450}{76.2\ X\ 5.28}\left(\frac{N}{mm^2}\right) = 11.05\ \text{MPa} \tag{32}$$

8. Data Reduction & Analysis

The plate was physically loaded such that its top edge was stationery while the bottom edge moved vertically downward. To simulate the top and bottom ends of the laminate being extended equally, the DIC-recorded displacement data in the loading (strong-stiff direction, vertical x) direction of Fig. 1 were post processed to be zero along the horizontal (x = 0) axis. Acknowledging the geometric

Table 1 DIC details.

Parameter	Equipment or setting
Cameras	The Grasshopper (Point Grey Research), model GRAS-50S5M-C
Imaging sensor	Sony ICX625 CCD, 2/3'' sensor format, 3.45 μm pixel size
Lens	CM 120 BK 15 COMPACT-0901 (focal ratio: 1.9 and focal length: 35 mm)
Sensor/digitization	2,448 × 2,048 at 15 FPS (framing rate)
Pixel to inch conversion	1 pixel = 0.05 mm
Subset, step sizes	21 and 8
Strain Resolution	50 microstrain

and mechanical symmetry about the x and y axes, Fig. 3 shows the resulting vertical displacements (u) throughout one quadrant.

From the displacement data of Fig. 3, n = 6,448 essentially equally spaced values of u were selected. Since DIC data at and near an edge are not reliable, no displacement information was employed within a distance 0.1R (= 1.27 mm) from the edge of the hole. In addition to the n = 6,448 DIC measured u-displacements, $\sigma_{xy} = 0$ was imposed at 3,601 equally spaced locations along x = 0, and $\sigma_{xy} = 0$ and v = 0 were similarly imposed at 3,601 equally located points along y = 0. A total of n + h = 6,448 + 3,601 + 3,601 + 3,601 = 17,251 side conditions (pieces of information) were used to evaluate the Airy coefficients, where n = 6,448 are DIC recorded u-displacement data and h = 10,803 represents the applied conditions.

From Eqs. (22), (23) and (28), one obtains

$$\begin{Bmatrix} u \\ \sigma_{xy} = 0 \\ v = 0 \end{Bmatrix}$$

$$= 2Re\left(\begin{bmatrix} p_1\zeta_1^j + p_2\left(C\zeta_2^j + B\zeta_2^{-j}\right) & i\left[p_1\zeta_1^j + p_2\left(C\zeta_2^j - B\zeta_2^{-j}\right)\right] \\ -\mu_1\dfrac{j\zeta_1^{j-1}}{\omega_1'(\zeta_1)} + \mu_2\dfrac{jB\zeta_2^{-j-1} - jC\zeta_2^{j-1}}{\omega_2'(\zeta_2)} & i\left[-\mu_1\dfrac{j\zeta_1^{j-1}}{\omega_1'(\zeta_1)} + \mu_2\dfrac{-jB\zeta_2^{-j-1} - jC\zeta_2^{j-1}}{\omega_2'(\zeta_2)}\right] \\ q_1\zeta_1^j + q_2\left(C\zeta_2^j + B\zeta_2^{-j}\right) & i\left[q_1\zeta_1^j + q_2\left(C\zeta_2^j - B\zeta_2^{-j}\right)\right] \end{bmatrix}\begin{Bmatrix} a_j \\ b_j \end{Bmatrix}\right) \tag{33}$$

$$= \begin{Bmatrix} Displacement\ data\ from\ DIC \\ Symmetry\ BC's(shear\ stress) \\ BC's(transverse\ displacements) \end{Bmatrix}$$

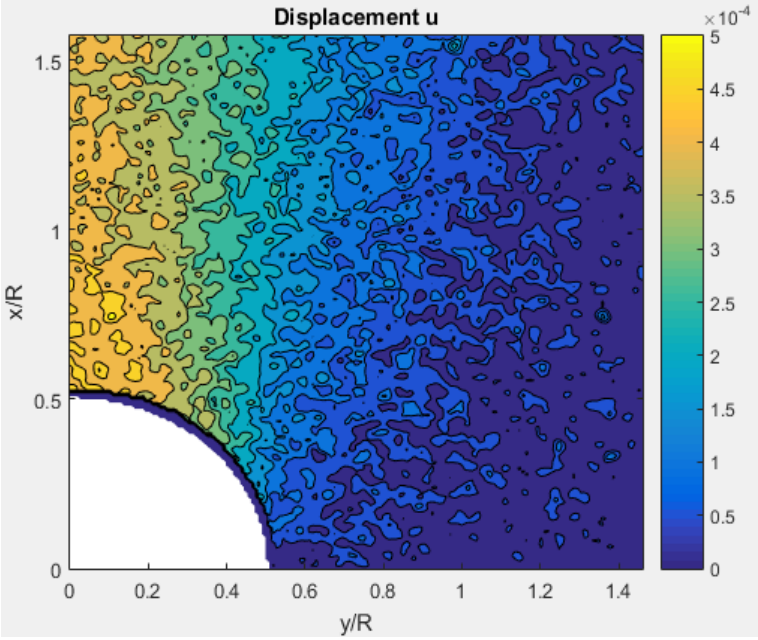

Fig. 3 DIC provided vertical displacements u in vertical loading direction x.

which can be written as:

$$[A]_{(n+h)*j}\{c\}_{j*1} = \{d\}_{(n+h)*1} \quad (34)$$

Matrix [A] depends on the material properties and the mapping function, vector {c} consists of the Airy coefficients and {d} includes the DIC recorded displacement data along with the imposed conditions. The only unknowns in the above equation are the Airy coefficients in vector {c} which can be evaluated from Eq. (34) by least square method. The backlash operator in Matlab was used to evaluate the unknown complex Airy coefficients.

A realistic number, *k*, of Airy coefficients to use in Eqs. (20)-(28) must be determined. Too few coefficients can produce inaccurate results, while too many coefficients can cause the Airy matrix, [A], of Eq. (34) to become unstable or even singular due to computer round-off errors. The number of Airy coefficients to utilize was determined by plotting the RMS (root mean square) of the difference between the magnitudes of the DIC-recorded u-displacements, {d}, with those predicted, {d'}, by Eq. (22) versus the number of complex coefficients, k [8].

Although that information suggested using $2 \leq k \leq 10$ would be reasonable, it is convenient to employ as few coefficients as acceptable. Moreover, comparing the measured and reconstructed (from Eq. (22)) displacements confirms the rational use of k = 2 complex coefficients (Fig. 4a). As the number of employed coefficients increases, the reconstructed displacements (Figs. 4b and 4c) start to deviate from the DIC-recorded data. For viewing convenience, Figs. 4-9 are plotted with the loading (x-direction) direction in the traditional horizontal orientation.

9. Results

Having evaluated the Airy coefficients, the displacements and stresses are available at, and in the neighborhood, of the hole from Eqs. (22), (23) and (26)-(28). The DIC-hybrid determined displacements and stresses are compared with FEM predictions in Figs. 5-10. Displacements are normalized with respect to the radius (R = 12.7 mm) of the hole and the stresses are normalized with respect to the far-field stress (σ_0 = 11.05 MPa). All experimental results are based on the DIC-recorded u-displacement data. The agreement between the DIC-hybrid and FEM results is excellent in Figs. 5-7, 9 and 10. Although Fig. 8 illustrates some discrepancy between the DIC-based and FEM results, the respective magnitudes are extremely small and the differences are inconsequential. The high quality of the v/R contours in Fig. 6 from recorded u-displacement information is noteworthy.

Reliability of the DIC-hybrid method was further evaluated by checking load equilibrium from the DIC-based stress σ_{xx} over horizontal areas of the loaded plate using Eq. (35):

$$F = \int_{-W/2}^{W/2} \sigma_{xx} dA = 2\int_{0}^{W/2} \sigma_{xx} t dy \quad (35)$$

where, t is the thickness and W is width. Using the trapezoidal rule of Matlab to compute the integration, this was evaluated at various locations of x (= 0, R, 1.3R, 1.5R, 1.7R, 2R, W/2). The computed load was found to be within 2% of the physically applied 4.45 kN (1,000 lbs) load at each of these locations.

10. Summary, Discussion and Conclusions

The individual stresses in a circularly-perforated, finite, orthotropic composite plate are reliably determined here from a single DIC-measured displacement field. The displacement information is synergized with a complex variable power series expansion of Airy stress functions, conformal mapping and analytical continuation. The need for only two complex Airy coefficients is noteworthy. Unlike finite element or theoretical/analytical analyses, the current method does not require knowing the applied loading. This is important as external loads are often unknown in practice. Virtually all theoretically stressed orthotropic members are restricted to infinitely large geometry. Moreover, unlike the present approach, prior DIC analyses of circularly-perforated

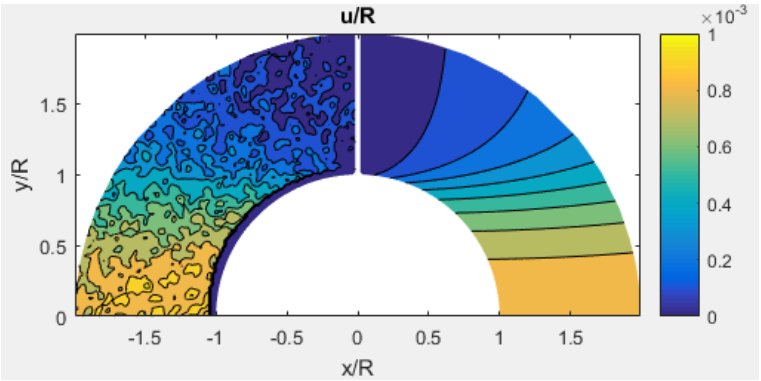

(a) k = 2

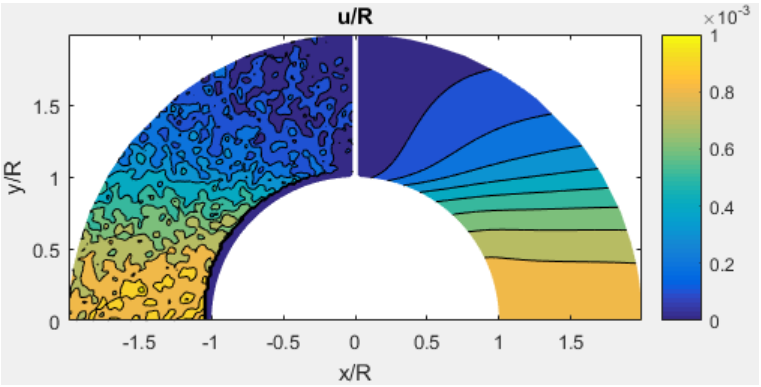

(b) k = 4

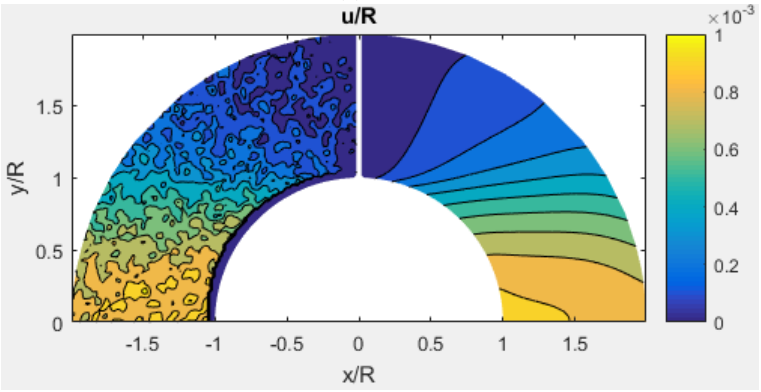

(c) k = 10

Fig. 4 Comparing u-displacement contours obtained from DIC (left side) with reconstructed (right side) from the complex hybrid analysis for n + h = 17,251 and k = 2, 4 and 10, respectively.

orthotropic composites necessitated measuring both in-plane displacements and did not provide reliable information at the edge of the hole [4, 5].

Most DIC approaches differentiate the measured displacements with schemes which lack any strong theoretical, analytical or mechanics basis. Such processes can give poor results [12]. This shortcoming is overcome here by processing the recorded displacement data with a stress function. One could measure displacements by other than DIC. However, the herein ability to need only one in-plane displacement field is significant. For example, obtaining both u and v by moiré, ESPI (electronic speckle pattern interferometry), grids or holography necessitates fairly complicated experimental setups or post-processing. Irrespective of which displacement-based technique is used, it is not unusual to have locations where one of the u or v is of poor quality.

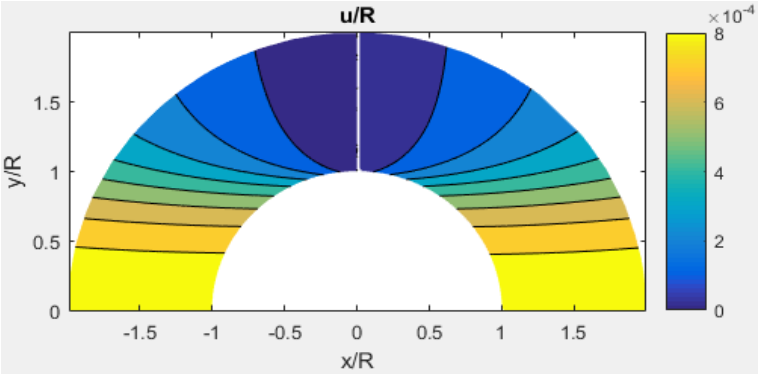

Fig. 5 Contours of u/R from FEA (left side) and DIC-hybrid method (right side) for k = 2, n + h = 6,448 + 10,803 = 17,251.

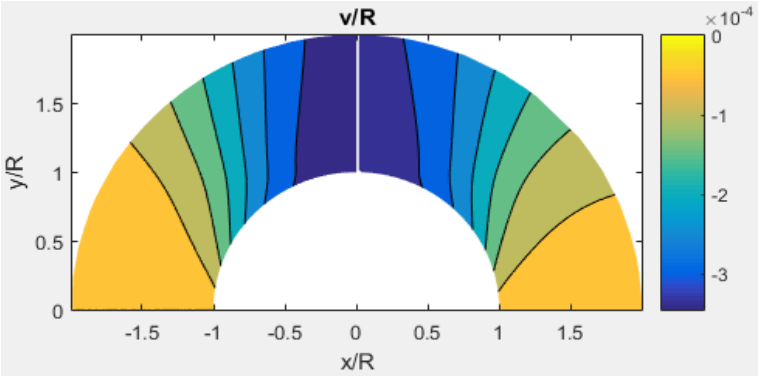

Fig. 6 Contours of v/R from FEA (left side) and DIC-hybrid method (right side) for k = 2, n + h = 6,448 + 10,803 = 17,251.

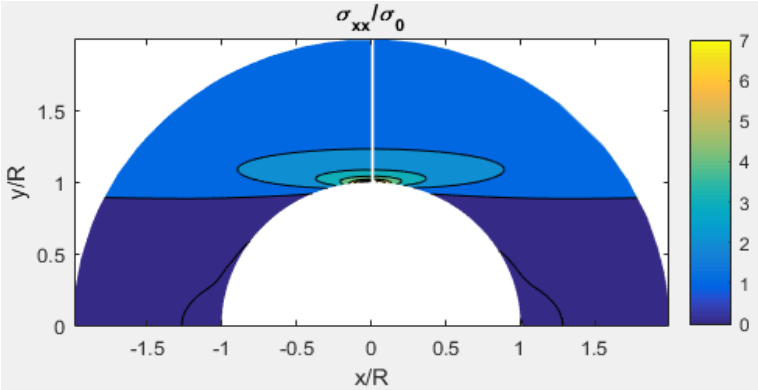

Fig. 7 Contours of σ_{xx}/σ_0 from FEA (left side) and DIC-hybrid method (right side) for k = 2, n + h = 6,448 + 10,803 = 17,251.

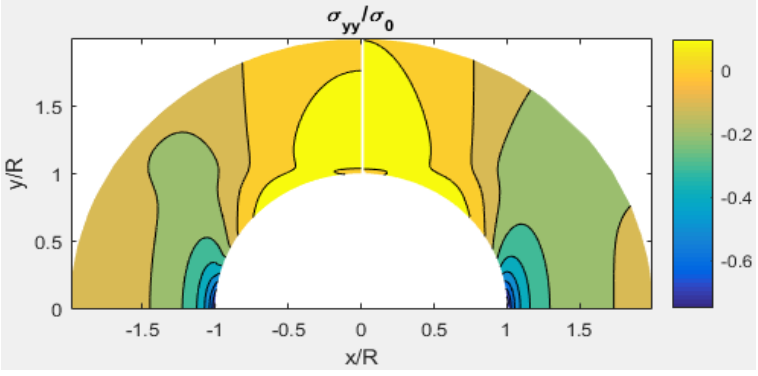

Fig. 8 Contours of σ_{yy}/σ_0 from FEA (left side) and DIC- hybrid method (right side) for k = 2, n + h = 6,448 + 10,803 = 17,251.

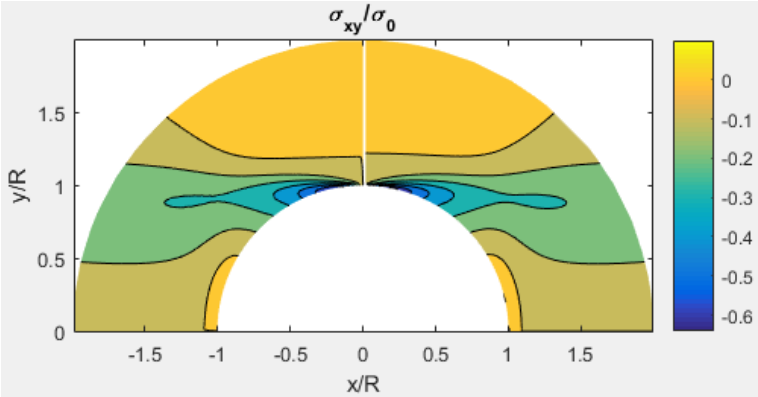

Fig. 9 Contours of σ_{xy}/σ_0 from FEA (left side) and DIC-hybrid method (right side) for k = 2, n + h = 6,448 + 10,803 = 17,251.

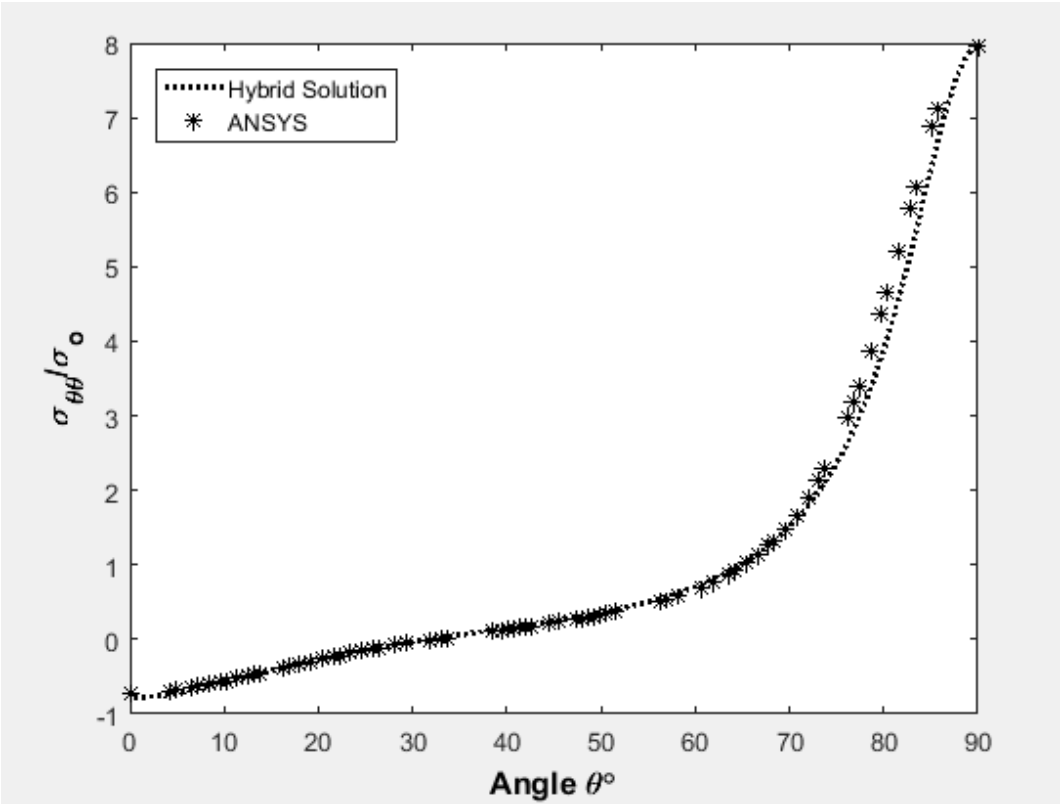

Fig. 10 Plot of $\sigma_{\theta\theta}/\sigma_0$ along the boundary of the hole from ANSYS & Hybrid analysis using k = 2 complex coefficients and n + h = 6,448 + 10,803 = 17,251.

The present technique simultaneously smooths the measured information, satisfies equilibrium and compatibility, and determines individual stresses full-field, including on the edge of the hole. Moreover, the approach is applicable to engineering problems involving multiple and/or non-circular geometric discontinuities, non-symmetrical situations, parabolic and/or deep notches, square holes with filleted corners, and highly complicated shapes using Schwartz-Christoffel concepts. Isotropic cases could be handled by numerically letting $E_{xx} \approx E_{yy} = E$, $\nu_{xy}=\nu$ and $G_{xy} = \frac{E}{2(1+\upsilon)}$.

Acknowledgments

Special thanks to Jacob Zeuske for his technical assistance and Michael Hughes for machining the composite plate.

References

[1] Pilkey, W. D., and Pilkey, D. F. 2008. *Peterson's Stress Concentration Factors*. New York: Wiley.

[2] Rowlands, R. E., Daniel, I. M., and Whiteside, J. B. 1973. "Stress and Failure Analysis of a Glass-Epoxy Composite Plate with a Circular Hole." *Exp. Mech.* 13 (1): 31-7.

[3] Rhee, J., He, S., and Rowlands, R. E. 1996. "Hybrid Moiré-Numerical Stress Analysis around Cutouts in Loaded Composites." *Exp. Mech.* 36 (4): 379-87.

[4] Lagattu, F., Brillaud, J., and Lafarie-Frenot, M. C. 2004. "High Strain Gradient Measurements by Using Digital Image Correlation Technique." *Mater. Charact.* 53 (1): 17-28.

[5] Ashrafi, M., and Tuttle, M. E. 2015. "High Strain Gradient Measurements in Notched Laminated Composite Panels by Digital Image Correlation." *Composite, Hybrid, and Multifunctional Materials* 4: 75-81.

[6] Lekhnitskii, S. G. 1968. *Anisotropic Plates*. New York: Gordon and Breach.

[7] Gerhardt, T. D. 1984. "A Hybrid/Finite Element Approach for Stress Analysis of Notched Anisotropic Materials." *J. Appl. Mech.* 51 (4): 804-10.

[8] Fatima, N. S. 2017. "Photomechanical Full-Field Stress Analysis of Isotropic and Orthotropic Materials Containing Various Cutouts." Ph.D. thesis, University of Wisconsin-Madison.

[9] Sutton, M. A., Schreier, H. W., and Orteu, J. J. 2009. *Image Correlation for Shape, Motion and Deformation Measurements Basic Concepts, Theory and Applications*. Springer.

[10] Correlated Solutions. Accessed April 21, 2016. [Online]. Available: http://www.correlatedsolutions.com.

[11] Pan, B., Xie, H. M., Wang, Z. Y., Qian, K. M., and Wang, Z. Y. 2008. "Study on Subset Size Selection in Digital Image Correlation for Speckle Patterns." *Opt. Express* 16 (10): 7037-48.

[12] Samad, W. A., Khaja, A. A., Matthys, D. R., and Rowlands, R. E. 2013. "Full-Field Recorded Displacements and Their Derivatives." In *Proceedings of the International Conference on Computational & Experimental Engineering and Sciences: Recent Advances in Whole-Field Displacement Measurement Techniques,* Seattle.